Observations of twinning in $YBa_2Cu_3O_{6+x}$, $0 < x < 1$, at high temperatures

2002 J. Phys.: Condens. Matter 14 9763

(http://iopscience.iop.org/0953-8984/14/41/331)

INSTITUTE OF PHYSICS PUBLISHING JOURNAL OF PHYSICS: CONDENSED MATTER

J. Phys.: Condens. Matter **14** (2002) 9763–9778 PII: S0953-8984(02)35648-0

Observations of twinning in $YBa_2Cu_3O_{6+x}$, $0 < x < 1$, at high temperatures

B Khoshnevisan[1,2], D K Ross[1], D P Broom[1] and M Babaeipour[1,3]

[1] Institute for Materials Research, University of Salford, Salford M5 4WT, UK
[2] University of Kashan, Kashan, Iran
[3] University of Bu-Ali-Sina, Hamadan, Iran

Received 9 April 2002
Published 4 October 2002
Online at stacks.iop.org/JPhysCM/14/9763

Abstract

We report here on the nature of the twinning associated with the tetragonal to orthorhombic I (T/OI) phase transition in YBCO, for temperatures between 500 and 600 °C. *In situ* neutron diffraction measurements show the coexistence of the T and split OI peaks in the vicinity of the transition. However, by direct numerical simulation, we show that this is to be expected from the twinned OI structure when the separation of adjacent twinning planes and the orthorhombicity both approach zero. It is demonstrated that the observed *hkl*-dependent peak broadening is consistent with this interpretation. A comparison of the measured and simulated peak shapes enables us to make an approximate estimate of the actual twin widths for a given orthorhombicity.

(Some figures in this article are in colour only in the electronic version)

1. Introduction

It is well known that, in the cuprate high T_c superconductors, the critical current density, J_c, and the flux lattice density Φ_B, are both largely determined by the microstructure as observed on a length scale of some 100 Å. Thus, for instance, the twinning microstructure in YBCO is found to influence the flux pinning effect, increasing J_c to values greater than 10^5 A cm^{-2} for magnetic fields of several teslas [1, 2]. This length scale is clearly within the range of electron microscopy and of diffraction profile shape analysis, as measured using either x-ray or neutron powder diffraction methods [3, 4] or by electron diffraction. Experimental measurements [5] and theoretical studies [6] both show that, for most applications, the microstructure of the cuprates is determined by the non-equilibrium treatments they have received during processing. This is not unwelcome, because it allows us to optimize the material through adjustment of the thermal history, in addition to any purely chemical changes. However, the process of optimization can only be modelled through a detailed understanding of the mechanisms involved. In this paper, we report on the equilibrium structure of the $YBa_2Cu_3O_{6+x}(0 < x < 1)$ system, measured *in*

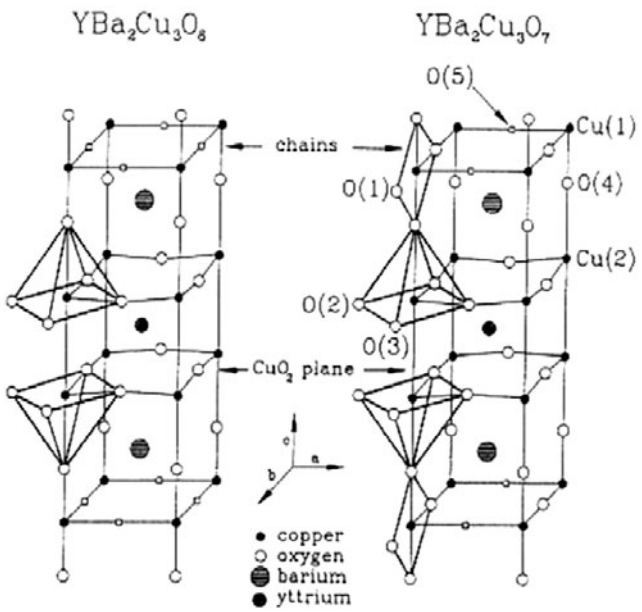

Figure 1. The unit cell of YBCO for the tetragonal phase (left) and the ortho I phase (right).

situ at high temperatures, from which different ambient structures can be produced by different cooling profiles.

In general, the most significant micro-structural feature observed on this length scale is the domain size of the twinning structure [7, 8]. This structure is produced as a result of the phase transition from the 'para-elastic' phase (a tetragonal structure, stable at high temperature and low oxygen concentration) to the 'ferro-elastic' phase (orthorhombic I, stable at lower temperatures and higher concentrations). The breaking of the symmetry generates elastic strains which, in turn, drive the formation of the twin domain structure. Following the approach of Landau phase transition theory, we would expect to be able to define an 'order parameter' in terms of the temperature, pressure and chemical composition of the sample that would quantitatively explain the transition process [9]. In the present paper, we examine the nature of this transition, as observed in conditions of thermodynamic equilibrium at temperatures around 600 °C where the relaxation to the equilibrium structure is conveniently fast.

The structures of the tetragonal and orthorhombic I phases are shown in figure 1. From experiment, the phase diagram is known in some detail, as a function of oxygen content and temperature [10]. The corresponding oxygen partial pressure (pp) isotherms are also well known [11, 12], so that the oxygen content (and hence the structure) can be determined by controlling the oxygen pp. Moreover, the remarkably simple lattice gas model of the Cu–O plane, due to de Fontaine *et al* [13], which assumes a repulsive interaction between nearest-neighbour oxygen atoms, an attractive interaction between second-nearest-neighbour oxygen atoms separated by a Cu atom and a repulsion between second-nearest-neighbour interactions not separated by Cu, describes the system well. Thus, when used to predict the phase diagram, either using the cluster variation method [14] or the Monte Carlo method [15], it produces an excellent match to the experimental data with the right structures (tetragonal, ortho I and ortho II phases) in roughly the correct parts of the (temperature–oxygen content) phase field.

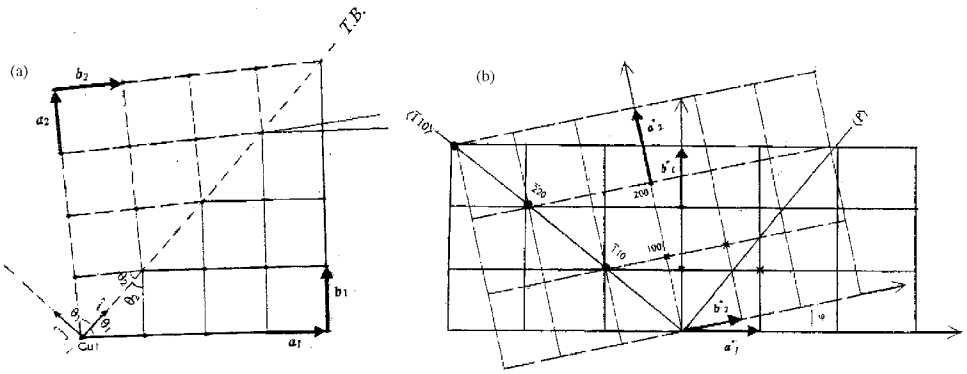

Figure 2. (a) Twinning in real space on the $(-1, 1, 0)$ plane (b) The reciprocal lattice produced by superimposing the reciprocal lattices of each twin. The rotation angle between the two reciprocal lattices is $\varphi = \tan^{-1} b/a - \tan^{-1} a/b$.

However, this model does not include the effects of lattice distortions caused by the fact that, in the Cu–O plane, the Cu–Cu distance is increased when these atoms are separated by an oxygen atom. This tendency produces a mismatch between the a and b parameters ($a < b$) in the orthorhombic phases as more oxygen atoms move from between the Cu–Cu bonds on the a to the equivalent position on the b direction. It is this local mismatch that produces the tweeding and twinning patterns seen in electro-micrographs at ambient temperatures [3] and also gives rise to some diffuse neutron scattering [16]. The tweeding pattern is seen in the tetragonal phase and corresponds to a short-ranged distinction between the a and b directions. At the phase transition, this correlation extends through the crystallite, uniquely defining its a and b directions. The twinning geometry in the basal plane is indicated in figure 2(a) and the corresponding reciprocal lattice for the twinned structure is shown in figure 2(b). Note that, if (as shown) the twinning plane normal is in the $\langle \bar{1}10 \rangle$ direction, the $(\bar{1}10)$ and, more generally the $(\bar{h}h0)$ reflections, are not split. Moreover, in the polycrystalline average, the (hhl) reflections will also coincide with each other, in that they lie on the same sphere of reflection.

At higher temperatures, the T/OI transition has been investigated under equilibrium conditions by Jorgensen *et al* [17] who measured the neutron diffraction patterns as a function of temperature under different fixed oxygen pressures. These authors demonstrated that the orthorhombicity disappeared in a continuous fashion as the system approached the phase boundary, implying a second-order transition. On the other hand, Rand *et al* [18] observed a region of co-existence of the T and the split OI reflections, which would normally be taken to imply a first-order transition. The objective of the present paper is to investigate whether twinning occurs at high temperatures and how its existence can be related to a second-order phase transition.

Thus, the normal expression for the distance between the twinned regions in an orthorhombic phase is that due to Khachaturyan [19, 20]:

$$T = [G\gamma/ES^2]^{1/2}. \tag{1}$$

Here T is the twin separation, γ is the twin boundary energy, G is the grain size, E is the elastic modulus and S is the orthorhombicity where it is assumed that the grain is elastically bound to the neighbouring grains having a different orientation. However, at high temperatures, we would expect that entropy effects would introduce fluctuations in the value of T about some mean value predicted from (1) above. We should note here that the micrographs of samples

showing twinned domains at ambient temperatures [7, 8], often show quite large and rather uniform values of T. We believe that these large domains are associated with particles that consist of a single crystallite so that they can completely transform with no elastic strain.

Now, if we assume that the difference between the occupation probability on the a and b directions is proportional to the orthorhombicity [17], we can calculate the twin boundary energy from the number of extra near-neighbour repulsions. Thus, in mean field theory, we must conclude that γ is proportional to S^2, from which it follows that T is independent of S [20]. However, the functional form of $\gamma(S)$ is probably more complex than this because, clearly, with so many vacant O sites, the local arrangement of oxygen atoms can produce a lower internal energy than that predicted by MF theory, by minimizing the number of nearest-neighbour interactions and also through some depletion in oxygen content near the twin plane [3, 21]. This flexibility will be greatest at lower values of S so that we would expect $\gamma(S)$ to increase as a higher power of S than S^2. Hence, we can conclude that the mean separation of the twin planes would tend to zero as S tends to zero. It is therefore of considerable interest to investigate the resulting diffraction pattern near this limit, to see if we can infer the variation of T from a diffraction measurement.

To the best of our knowledge, previous authors have implicitly assumed that the diffraction pattern from a twinned crystal would be just the superposition of the two separate diffraction patterns from each twin volume as indicated by the twin reciprocal lattice points in figure 2(b). However, the observations of Locherer *et al* [9] on single crystals of substituted YBCO systems at room temperature, where substitution allows one to approach the phase boundary in a continuous way, showed that quite complex peak shapes are observed which include intensity at the centre of a cluster of twinned peaks. Indeed, it is obvious that the assumption that the separate peak intensities can be summed will break down when there is significant interference between the scattering from two adjacent twins. The condition for this to happen is that the scattered wave from atoms in the middle of a twinned region will have a phase that is within π radians of the wave scattered from the equivalent atom in the absence of twinning. This will clearly happen in the limit of small orthorhombicity and small twin widths. In section 2 below, we present an analytical model for the phase difference in the scattering between different twins. We then describe a numerical simulation of the diffraction pattern to be expected for the (200) and (020) reflections and indicate how this behaviour is reproduced for other reflections. Then, in section 3, we describe our *in situ* neutron diffraction measurements. These were taken at intervals along the oxygen absorption/desorption isotherms at 500, 550 and 600 °C. Finally, in section 4, we present the experimental results and, by comparing the predictions with the observations, show that the transition is indeed second order, where the width of an individual twin and the orthorhombicity both go to zero at the phase boundary. We also show that the hkl dependence of the peak widths is consistent with this analysis.

2. The model

The geometry of the twinning in YBCO is shown in figure 2(a). The orthorhombicity is defined by the parameter, S, where $S = 2(b-a)/(a+b)$. The actual positions of the lattice points in real space are best defined in terms of Cartesian co-ordinates x, parallel to the twin boundary, and y, normal to the boundary, with corresponding unit vectors $\boldsymbol{i}$ and $\boldsymbol{j}$. Here, the orientation of the original lattice is given by lattice vectors $\boldsymbol{a_1}$ and $\boldsymbol{b_1}$ and the twinned lattice by the vectors b_2 and $\boldsymbol{a_2}$ where

$$\begin{aligned} \boldsymbol{a_1} &= a\cos\theta_1\boldsymbol{i} - a\sin\theta_1\boldsymbol{j} \qquad \text{and} \qquad \boldsymbol{b_1} = b\sin\theta_1\boldsymbol{i} + b\cos\theta_1\boldsymbol{j} \\ \boldsymbol{a_2} &= a\cos\theta_1\boldsymbol{i} + a\sin\theta_1\boldsymbol{j} \qquad \text{and} \qquad \boldsymbol{b_2} = b\sin\theta_1\boldsymbol{i} - b\cos\theta_1\boldsymbol{j}. \end{aligned} \tag{2}$$

Now, the displacement of an atom in the first plane of the twin, compared to where it would be in the absence of twinning, will be

$$\begin{aligned} \boldsymbol{D} = (\boldsymbol{b_2} - \boldsymbol{a_1}) &= (b\sin\theta_1 - a\cos\theta_1)\boldsymbol{i} - (b\cos\theta_1 - a\sin\theta_1)\boldsymbol{j} \\ &= (b^2 - a^2)/\sqrt{(a^2 + b^2)}\boldsymbol{i}. \end{aligned} \tag{3}$$

In general, the displacement in the Tth plane from the twin boundary is $\boldsymbol{D_T} = T\boldsymbol{D}$. Turning to the reciprocal lattice, the two sets of lattice vectors are now $\boldsymbol{a_1^*} = 2\pi\boldsymbol{a_1}/a^2$, $\boldsymbol{b_1^*} = 2\pi\boldsymbol{b_1}/b^2$, $\boldsymbol{a_2^*} = 2\pi\boldsymbol{a_2}/a^2$ and $\boldsymbol{b_2^*} = 2\pi\boldsymbol{b_2}/b^2$. The reciprocal lattice vectors for h, k and h', k' reflections in each of the twinned lattices are respectively $\boldsymbol{Q}_{hk}$ and $\boldsymbol{Q}_{h'k'}$ where

$$\boldsymbol{Q}_{hk} = h\boldsymbol{a_1^*} + k\boldsymbol{b_1^*} \qquad \text{and} \qquad \boldsymbol{Q}_{h'k'} = h\prime\boldsymbol{b_2^*} + k\prime\boldsymbol{a_2^*}. \tag{4}$$

For a given pair of reflections, with $h = h'$ and $k = k'$, the separation will be

$$\begin{aligned} \boldsymbol{Q}_{hk} - \boldsymbol{Q}_{h'k'} &= h(\boldsymbol{a_1^*} - \boldsymbol{b_2^*}) + k(\boldsymbol{b_1^*} - \boldsymbol{a_2^*}) = 2\pi h[(\cos\theta_1/a - \sin\theta_1/b)\boldsymbol{i} \\ &\quad + (\cos\theta_1/b - \sin\theta_1/a)\boldsymbol{j}] + 2\pi k[(\sin\theta_1/b - \cos\theta_1/a)\boldsymbol{i} \\ &\quad + (\cos\theta_1/b - \sin\theta_1/a)\boldsymbol{j}] = 2\pi(h + k)(a^2 - b^2)/[ab\sqrt{(a^2 + b^2)}]\boldsymbol{j}. \end{aligned} \tag{5}$$

As expected, the displacement is in the $-\boldsymbol{j}$ direction and goes to zero when either $a = b$ or when $h + k = 0$.

Now the phase difference in the scattering from two points $\boldsymbol{r}$ apart at wavevector transfer $\boldsymbol{Q}$ is $\Phi = \boldsymbol{Q}\cdot\boldsymbol{r}$. Hence the phase difference due to twinning at the Tth plane from the twinning plane, when evaluated for the (h, k) reflection of the untwinned lattice, will be $(\boldsymbol{Q}_{hk}\cdot T\boldsymbol{D})$

$$\Phi = (ha_1^* + k\boldsymbol{b_1^*})[T(b^2 - a^2)/\sqrt{(a^2 + b^2)}]\boldsymbol{i} = 2\pi(h + k)T(b^2 - a^2)/(a^2 + b^2) \tag{6}$$

for YBCO: $a \approx b \approx (a + b)/2$. So: $\Phi \approx 2\pi(h + k)TS \approx \pi$ for interference.

Hence interference will occur where

$$T \sim 1/\{2(h + k)S\}. \tag{7}$$

If the phase difference $\sim\pi$, the reflection at the position of one twin lattice point will interfere destructively with the reflection from the other twin and the interference region will appear between the twin reflections. This path difference will occur at higher T as S gets smaller. Furthermore, for a given S, the condition is satisfied for progressively smaller T as $(h + k)$ increases. For $\Phi \gg \pi$, the scattering from one twin will be essentially incoherent with that from the other twin while for $\Phi \ll \pi$ the waves from each twin are essentially in phase with each other and so one gets a single reflection at the average position with a width that depends on the total number of planes in the crystallite.

In order to be more quantitative about the structure of the reflected intensity, we have performed numerical calculations of the diffracted intensity distribution for a twinned atomic arrangement. In a realistic model, the wall thickness between adjacent twins would probably be some ångstroms thick (and this would correspond to some continuous change in the oxygen order across the twinning plane and a related continuous change in the a and b lattice parameters). However, it is clear that the assumption here—that the twinning is completed in a single plane—will not significantly affect the calculated shape of the Bragg reflections, because the effect of a finite twin wall thickness would be merely to create additional broad diffuse scattering extending between the Bragg reflections [9]. Also, as pointed out above, we would expect the positions of the twinning planes to show statistical fluctuations at higher temperatures. However, such fluctuations would just have the effect of smoothing the calculated shapes.

The scattering function, $S(\boldsymbol{Q})$, is calculated in 2D first for the *single-crystal representation* (scr), using the following expression:

$$S(\boldsymbol{Q}) = \frac{1}{N}\sum_i \sum_j \langle \exp\{\mathrm{i}\boldsymbol{Q}\cdot(\boldsymbol{r}_j - \boldsymbol{r}_i)\}\rangle. \tag{8}$$

Here $\boldsymbol{Q}(= Q_x\boldsymbol{i} + Q_y\boldsymbol{j})$ is the scattering vector in the basal plane, N is the total number of cells in the basal plane and the $\boldsymbol{r}$ vectors represent the positions of the cell corners (the Cu atoms). There is no need to model the actual atomic positions within the unit cell as we are not interested in predicting the structure factor, merely the peak shape. The corresponding $S(Q)$ for a *powder pattern representation* (ppr) can then be determined by integrating $S(\boldsymbol{Q})$ over a circle of constant Q.

In this model, we assume the length of the twinning plane (perpendicular to the twin separation) to be L unit cells (parallel to $\langle 110\rangle$), i.e. $N = L \times T$. The general behaviour of the diffraction features can be inferred from the contour plots shown below for the [200], [020] reflection pair. In these plots, T is kept constant while S is varied. For $T = 50$ and $L = 100$, figure 3(a) shows the [200] peak for the case of $S = 0$ (or $a = b$, the tetragonal case) in the scr. Here, the intensity pattern is in the form of a cross with a strong central peak. Consequently, the corresponding powder pattern only shows a single peak with low intensity wings. As S increases by stages (figures 3(b)–(e), $S = 0.003, 0.008, 0.013, 0.018$), the [200] and [020] patterns gradually resolve themselves into the first three peaks, with a central peak corresponding to a tetragonal peak and a pair of peaks on either side corresponding to the twinned orthorhombic regions. Further increase in S causes the central peak to shrink and disappear, leaving two separate peaks (consistent with the superposition of the diffraction peak for each individual twin as in figure 2(b)). The three peak structure in the transition region is clearly due to the interference between the waves diffracted from the two twins. The separation of the peaks is also proportional to S while the width of the peak normal to the twinning plane (Q_x) is proportional to $1/T$ (with its width parallel to the plane, (Q_y) being proportional to $1/L$). It is clear that the ppr version will also evolve from a single peak to a triple peak to a double peak. The additional modulation in the calculated contours comes from the harmonics generated by the twins and would presumably be averaged out in practice by statistical fluctuations in the twin separations. It should be noted that the central peak only appears where the broadened peaks from the individual twinned regions would overlap. The implication of the above argument is that the form of the pattern is determined by the term $(h + k)(S \times T)$. For $(h + k)(S \times T) \ll 1$, we get a single peak and for $(h + k)(S \times T) \gg 1$ we get two peaks. Further, the central peak and the split peaks appear with about the same intensity when $(h + k)(S \times T) \sim$ (a constant of the order of 1.0). The above calculations were performed for a pair of periodic structures twinned relative to each other. The calculation has been repeated for two alternating pairs of twinned regions for the case of $S = 0.018$ and $T = 50$ and 70. In this case, the peaks from each twin are split into two. This is because the phase from the planes in the third region will have been shifted by π compared to where they would be in the absence of twinning at the reciprocal lattice point for that twin, i.e. the diffraction from the two regions exactly cancel each other out.

Thus, as we move away from the perfect Bragg condition for this twin orientation, the phase difference changes from π. We thus see two peaks within the original envelope for a single twin. For extended sets of twins of fixed spacing, clearly the intensity would resolve itself into a set of satellites at positions where the phase difference for each twinned region is $2n\pi$. However, in practice, the twin separation will fluctuate about some mean value and so these effects due to interference between different twins in the same orientation will average out, leaving the above patterns as for a single pair of twins.

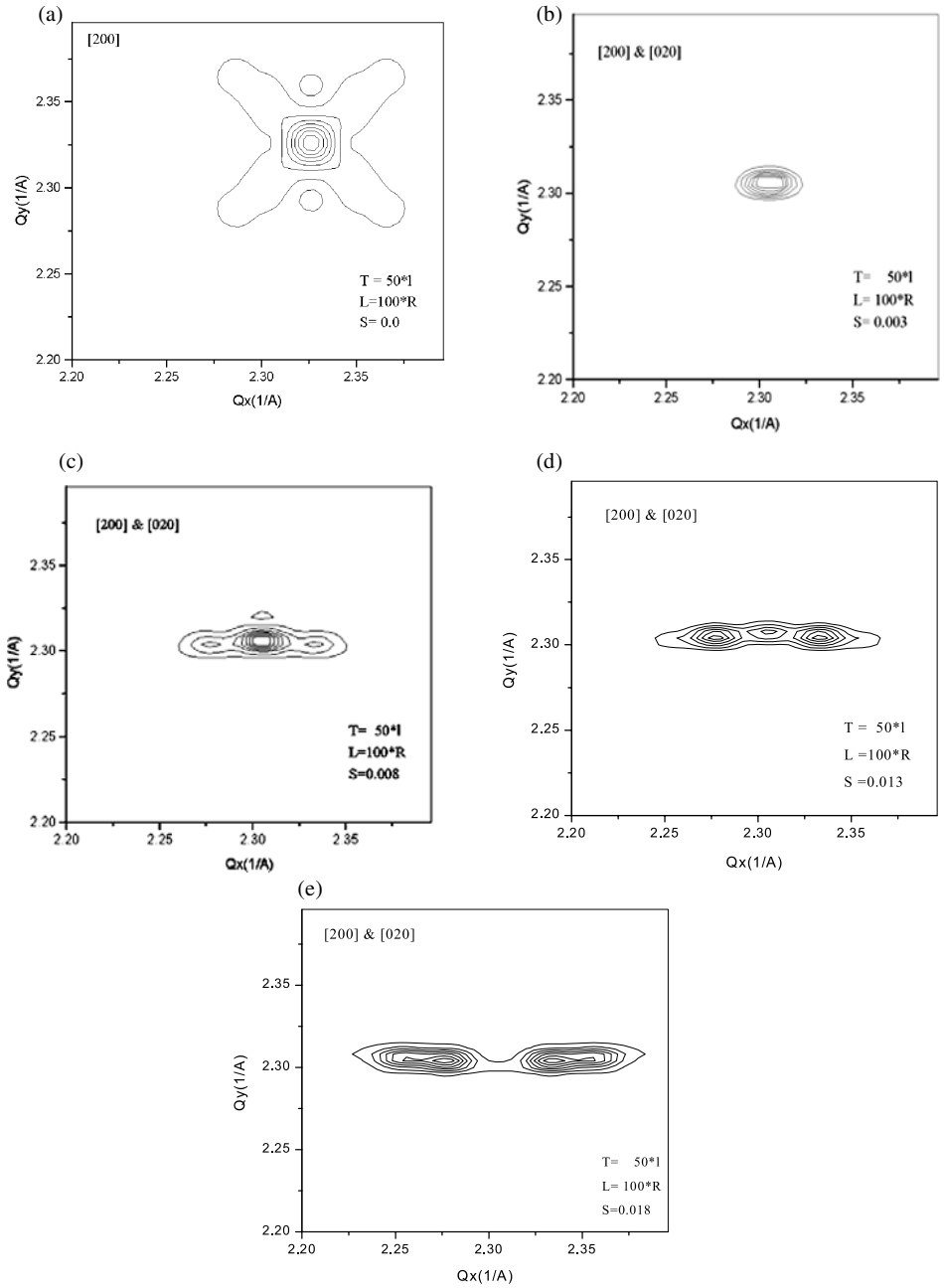

Figure 3. (a) $S = 0$. A single peak with butterfly wings (tetragonal symmetry). (b) $S = 0.003$. The peak becomes oval. (c) $S = 0.008$. Side peaks begin to develop. (d) $S = 0.013$. Side peaks rise above central peak. (e) $S = 0.018$. The twin peaks become separate.

Calculations have also been performed for other twinned reciprocal lattice points and similar results were obtained except that the appearance of the central peak scales differently with S and T. How this happens is easily understood from the positions of the twinned reflections as shown in figure 2(b). As expected, for large $S \times T$, the reflections are as

for superposition of the reflections from each twin, i.e. the width of each peak is inversely proportional to T and the reflections from each twin are separated in proportion to S. Interference effects are only to be expected if these independent peaks begin to overlap. Thus, if we go out to the nth-order reflection, the separation of the twinned reflections will increase by a factor of n, and so we would have to reduce T by a factor of n get the same pattern as in the fundamental.

Two important conclusions can be drawn from these figures. The first is that, as S and T tend to zero, a central peak begins to grow and eventually replaces the side peaks. Thus, the simultaneous observation of a split peak co-existing with a central peak does not necessarily indicate the simultaneous existence of the OI and T phases, i.e. it is not inconsistent with the transition being second order. The second point is that this situation can be identified by observing that the central peak tends to disappear as one goes to higher-order reflections, whereas, for a first-order transition, the central peak would remain with constant relative intensity for all orders.

We would note that we have recently completed a full analytical study of the diffraction from narrow twins which completely confirms the above results [22].

3. Experimental method and results

The measurements reported here are part of an extensive series of *in situ* neutron and x-ray powder diffraction measurements on this system in the temperature range from 200 to 600 °C made under controlled oxygen pressures. The objective of the measurements was to elucidate the equilibrium phase diagram, to characterize the superstructures in the lower part of the temperature range (orthorhombic II), to understand the equilibrium microstructures, in particular twinning, at higher temperatures and to establish the rate at which equilibrium is approached at different temperatures. Here, we will only consider the effects of twinning on the powder diffraction patterns which were collected in the higher temperature range (500, 550, 600 °C), and for oxygen pps in the range from 0.05 to 750 mbar. Other results will be presented elsewhere.

The polycrystalline samples used were supplied by PI-KEM[4] with a quoted oxygen content of $1.00 > x > 0.99$ and this oxygen stoichiometry was confirmed both by x-ray profile refinement and by the use of an intelligent gravimetric analyser (IGA)[5]. The particle size was specified to be between 1.5–5.0 μm and this was confirmed using scanning electron microscopy, which also suggested that each particle consisted of a number of distinct crystallites. The oxygen content was adjusted by varying the oxygen pps at given temperatures, with reference to previously measured isotherms [11, 12].

The neutron diffraction data presented here were obtained using the OSIRIS spectrometer at ISIS. The data were collected using the high resolution detector bank which yields a resolution of 0.3% in d spacing. This resolution was confirmed using a standard sample of silicon powder which was known not to broaden the diffraction peaks. The sample was placed in a quartz sample tube inside the furnace and this tube was connected to an oxygen supply at controlled pressures. The neutron data were collected for the d-spacing range of 1.2–12.0 Å at a series of predetermined oxygen pressures. For each of these pressures, a series of short diffraction measurements were first recorded until the pattern stopped changing, implying that thermodynamic equilibrium had been achieved. The full spectrum was then recorded over a period of two hours. The oxygen pressure was then changed and the procedure was repeated.

[4] PI-KEM Ltd, 6 Greenhill Rd. Camberley, Surrey GU15 1PE, UK.
[5] HIDEN Analytical Ltd, Gemini Business Park, Warrington WA5 5UN, UK.

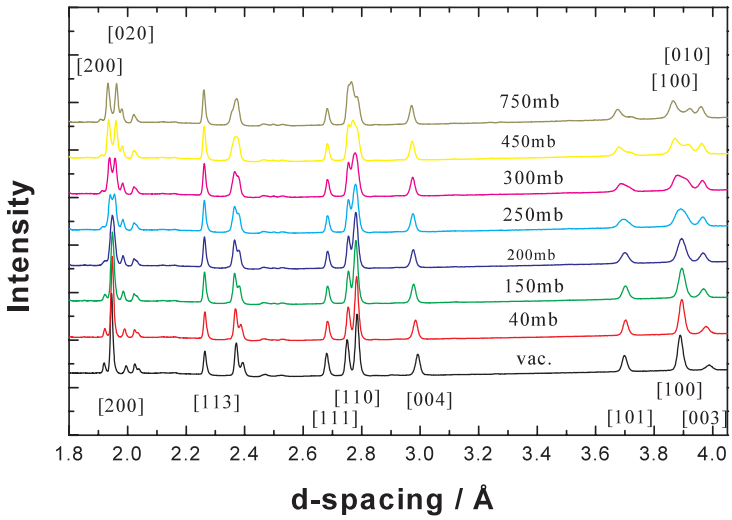

Figure 4. Neutron diffraction patterns measured at 600 °C under different oxygen pps.

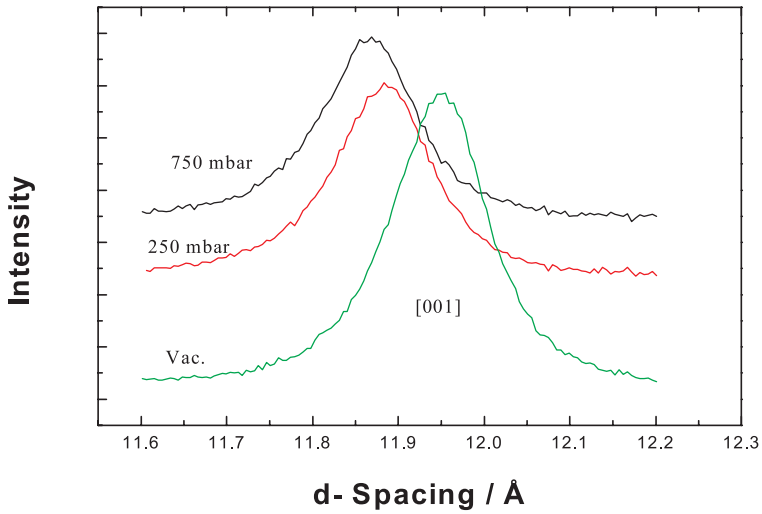

Figure 5. The displacement and broadening of the [001] peak with increasing oxygen pp through the T/OI transition.

The oxygen stoichiometry of the sample could thus be precisely controlled, using the known isotherm data.

Figure 4 shows how the most important peaks in the neutron diffraction patterns for 600 °C evolve as the oxygen concentration, x, is increased, starting in the T phase and passing through the T/OI phase transition region to the OI phase. Figure 5 shows the lattice contraction and associated peak broadening of the (001) peak ($d_{001} \sim 12$ Å) as x is increased at this temperature. This broadening in the (00l) direction is directly linked to the local stress caused by the reduction in the c parameter when the oxygen atoms in the Cu–O plane accumulate in the b direction. Similar sets of data have been acquired for a similar range of oxygen pressures at 500 and 550 °C.

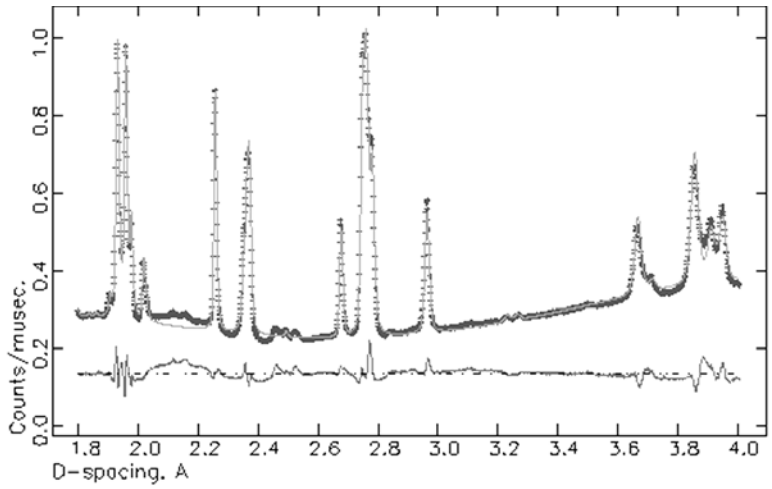

Figure 6. The GSAS full profile refinement for the sample in the OI phase in equilibrium with 750 mbar oxygen pp and 600 °C ($R_p = 0.028$). The poor fit is due to the *hkl*-dependent line broadening.

Because of the complex overlapping peaks profiles in the low d-spacing region (<2 Å), we will consider only the higher d-spacing range. A full profile refinement package such as GSAS would normally be employed for the analysis of peak broadening but, because of the strongly (hkl)-dependent peak-broadening effects caused by the twinned microstructure, this approach has not proved very satisfactory for YBCO (as shown in figure 6) [3, 4]. Thus, we have adopted the alternative method of independently analysing each line in the relevant d-spacing range. Here, although each TOF line is, strictly speaking, a convolution of the asymmetrical neutron pulse function with a pseudo-Voigt function (to reproduce the other instrumental and sample-dependent effects)—and this indeed reproduces the diffraction peaks of the standard sample (Si powder) when fitted with GSAS—the observed peaks for the YBCO samples are sufficiently broadened for the asymmetry in time-of-flight (TOF) to be unobservable. Therefore for the individual peak analysis used for the YBCO data, we have adopted the pseudo-Voigt parameters that came from the full profile refinement of the standard sample to deconvolute the instrumental broadening from the total broadening. This process shows that the sample broadening is essentially Gaussian. The broadenings quoted below are therefore the sample broadening after the deconvolution of the instrumental contribution.

Figure 7 shows a Williamson–Hall plot of the sample-dependent contribution to the broadenings of a sequence of peaks on a Q scale, for the measurement at 750 mbar oxygen pp and 600 °C—which is well into the OI phase ($x \sim 0.78$). The widths plotted are from fits to the individual peaks and also from a forced GSAS fit to the whole spectrum, ignoring the *hkl* dependence in the peak widths. The instrumental broadenings for the standard sample, also shown, were obtained from a GSAS fit performed as described above. It will be seen that the instrumental broadening is more or less independent of Q. On a TOF instrument, the time uncertainty due to the moderator is proportional to time, i.e. $\Delta d/d$ is independent of d, and hence ΔQ should increase linearly with Q. However, on OSIRIS, there is a further contribution to the resolution due to the wavelength dependence of the critical angle in the incident neutron guide, i.e. $\Delta\theta \sim \sqrt{\lambda}$. This term will tend to reduce ΔQ as Q increases and hence the overall broadening is more or less independent of Q. It is clear that the individual fits to the [110] and [220] reflections from our sample show sample-dependent broadenings

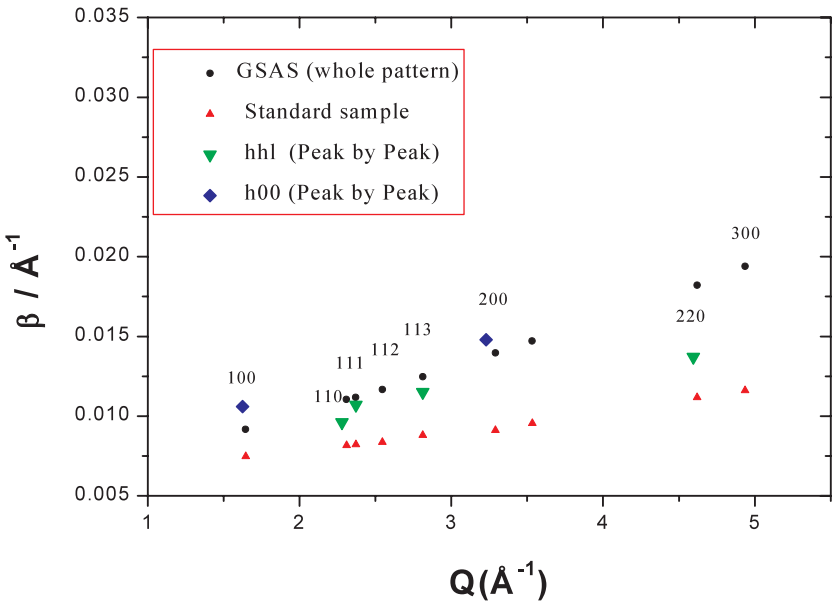

Figure 7. A Williamson–Hall plot of the peak widths in Q space for the data at 600 °C and 750 mbar oxygen pp.

comparable to the instrumental resolution which appear to be independent of Q, whereas the [h00] reflections are substantially broadened, with broadening increasing with Q. This is clear evidence that [110] twinning is present at this temperature. The extra broadening seen in the [111] and [113] reflections is clearly due to limited crystallite size or strain effects in the c direction. It will be noted that the broadening for the [200] peak is substantially greater than that for the [100] peak and a rough extrapolation to $Q = 0$ would suggest that little of this is due to finite size effects. The simultaneous GSAS fit, ignoring the anisotropy, also shows a general increase in the peak width with Q, suggesting that the broadening is dominated by strain effects caused by the changes in the bond lengths depending on the O positions.

Figure 8 presents the evolution of the individual peak widths measured after the sample was equilibrated at successive oxygen pps (and therefore at successive S values) while going from the tetragonal to the orthorhombic phase. When the sample is in the tetragonal phase (<150 mbar; $S = 0$), the peak widths generally increase with the order of reflection. However, after the transition ($S > 0$), as the sample absorbs more oxygen, the [110] peak become narrower—suggesting a reduction in strain effects as the twinning becomes established, while the [100] peaks become broader as expected from the model above. The variation in the [100] peak width during the absorption of oxygen can be explained by the appearance of twins with increasing in S. The peak width first increases due to the onset of twinning and then flattens.

We have recorded similar neutron data in further *in situ* neutron experiments at 500 and 550 °C. Figure 9 shows the equivalent data for 500 °C. Here, the noticeable difference is the increasing of the [110] peak width at higher orthorhombicity values ($S > 0.01$). It is possible that this is caused by stress due to the build-up of short-range order within the OI phase as the temperature is reduced.

In figure 10, we plot the variation of the fitted lattice parameters as a function of x at 600 °C. By extrapolating the a and b values, we can infer that the transition is close to $x = 0.59$, consistent with other data [11, 12]. The shape of the approach to the transition differs somewhat

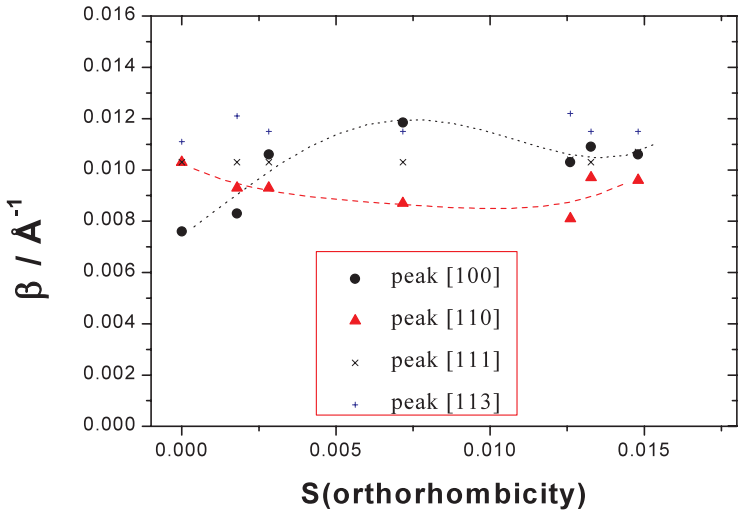

Figure 8. Variations of the peak widths in reciprocal space as a function of the orthorhombicity measured at 600 °C. The dotted and broken curves are a guide to the eye for the [100] and [110] peaks, respectively.

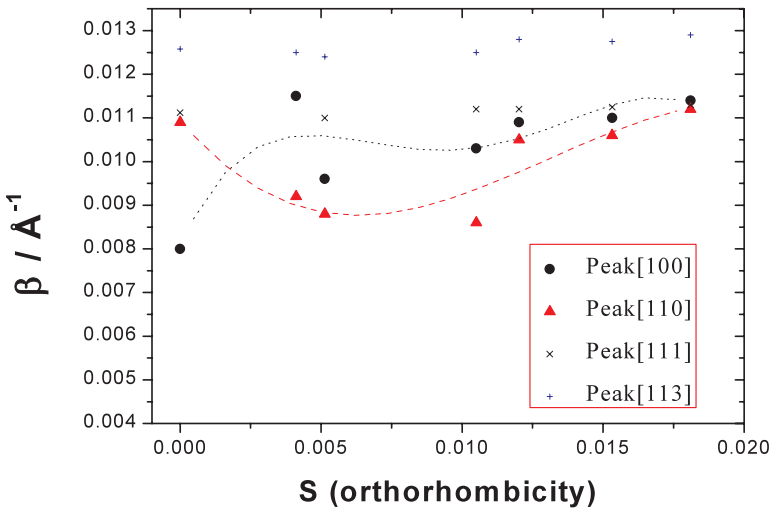

Figure 9. Plots of individual peak widths for a series of diffraction patterns recorded for increasing orthorhombicity at 500 °C. The dotted and broken curves are a guide to the eye for the [100] and [110] peaks, respectively.

from Jorgensen *et al*'s data. Figure 11 shows the variation of the site occupancies (O1 and O5), obtained from the full profile refinement. Here again, the results are consistent with the onset of orthorhombicity being in the vicinity of $x \sim 0.59$. Of necessity, the occupancy values come from a GSAS fit which only approximately describes the [100] and [010] shape and consequently the form of the curve is closer to that followed by the Jorgenson *et al* data.

Finally, in figure 12, we show how the oxygen pp varies across the phase transition at 600 °C. The oxygen occupation is obtained from full profile refinements of data from the 600 °C isotherm. Also shown is the variation in total oxygen content with pp measured

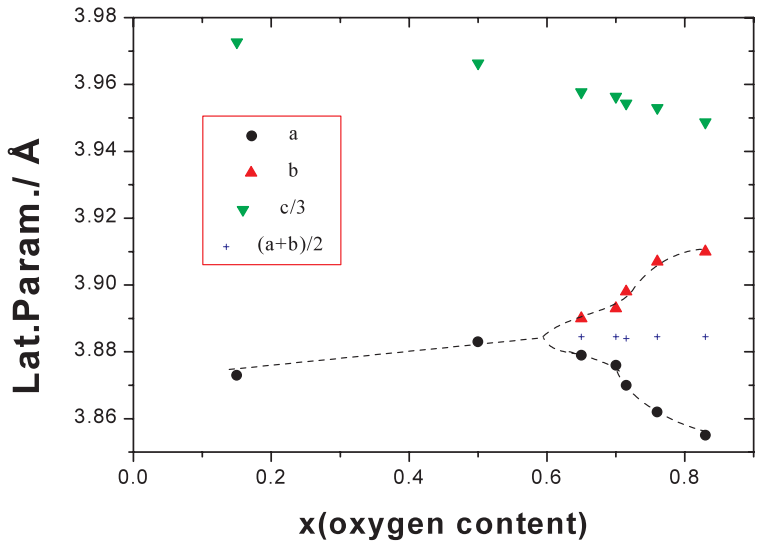

Figure 10. The fitted lattice parameters at 600 °C as a function of x. The intercept of dotted curves suggests the value of x for the T/O transition. The dotted curves are a guide to the eye.

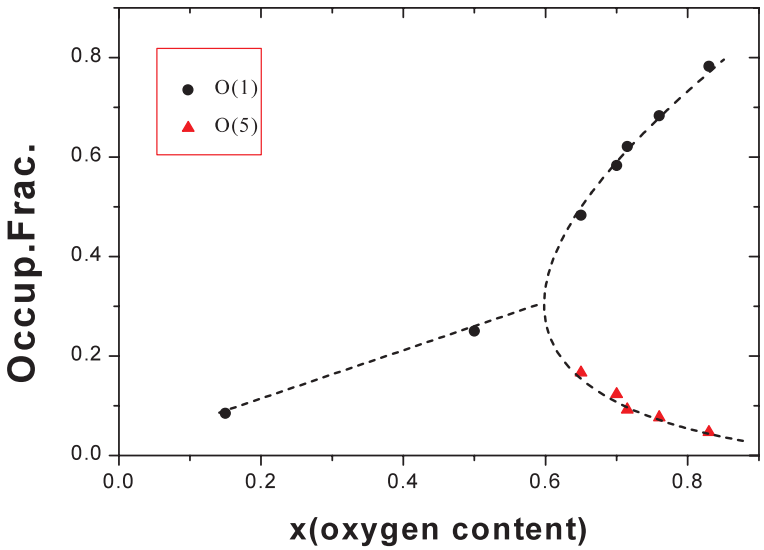

Figure 11. The variation in the fitted occupation fractions on the O(1) and O(5) sites at 600 °C. The bifurcation shows the estimated oxygen content at the phase transition. The dotted curves are a guide to the eye.

directly using the IGA technique. The discrepancy in the oxygen concentrations could be due to the difficulty in fitting the *hkl*-dependent broadening or to the transfer of scattering to diffuse scattering from disordered oxygen. Both techniques show the pressure variation to be continuous, with a smooth tangent across the phase transition, consistent with the theory of a second-order transition in a lattice-gas system [11, 12].

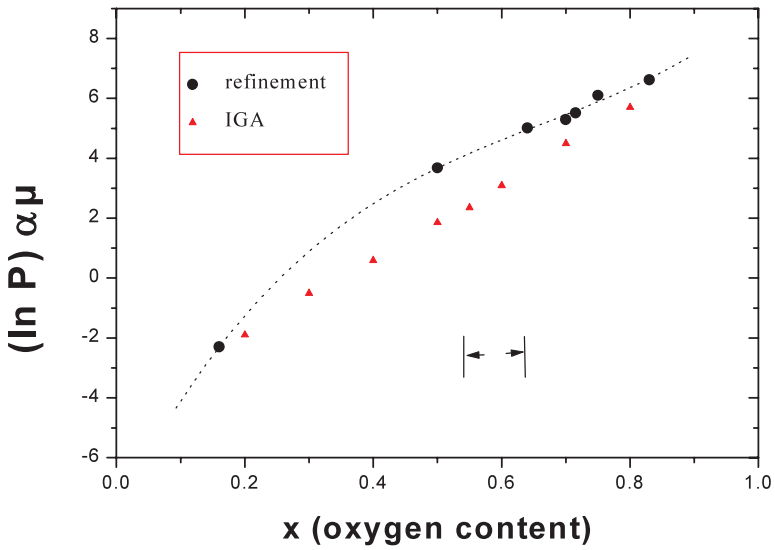

Figure 12. Variation of the oxygen pp at 600 °C plotted against the value of x determined from (a) the GSAS fits to the isothermal diffraction patterns and (b) direct measurements using the IGA method [12]. The interval marker shows the phase transition region.

We will now consider how the calculated ppr pattern (section 2) corresponding to different $S \times T$ values can be compared with diffraction data over the range of existence of the central peak. This comparison can be used to estimate the twin spacing, T, at least for the early stages after the transition. In practice, we do not observe a well-defined central peak but must infer its existence because of the need to include a third peak in the fit.

In figure 13(a), we show the diffraction pattern over the [200] and [020] peaks measured at 500 °C under 10 mbar oxygen pp which gives a value of $S = 0.011$ (when individually fitted by Gaussian profile shape). In figure 13(b), we show the corresponding numerical simulation for $S = 0.013$ and $T = 50$. Although the agreement is not perfect, it is clear that the data suggests that $T \sim 50$ for this temperature and pressure.

4. Conclusion

In this work, we have simulated the line broadening to be expected from a twinned system as the number of planes in each twin and the orthorhombicity both approach zero. We then analysed the observed diffraction peak shapes for YBCO measured in equilibrium as a function of oxygen pp and showed that the observed broadening was consistent with the model that the lattice is twinned in the $(\bar{1}10)$ plane in the orthorhombic phase and that the number of lattice planes in each twin increases from zero as the T/OI phase boundary is crossed, consistent with a second-order transition.

The main conclusions of this paper are:

(a) Diffraction from a sequence of narrow twinned regions can show a diffraction pattern that looks like a mixture of orthorhombic and tetragonal phases so that care must be exercised in concluding that there is a two-phase region in the phase diagram.
(b) The measured [*hh*0] reflections always remain much narrower than the other reflections, consistent with (110) twinning.

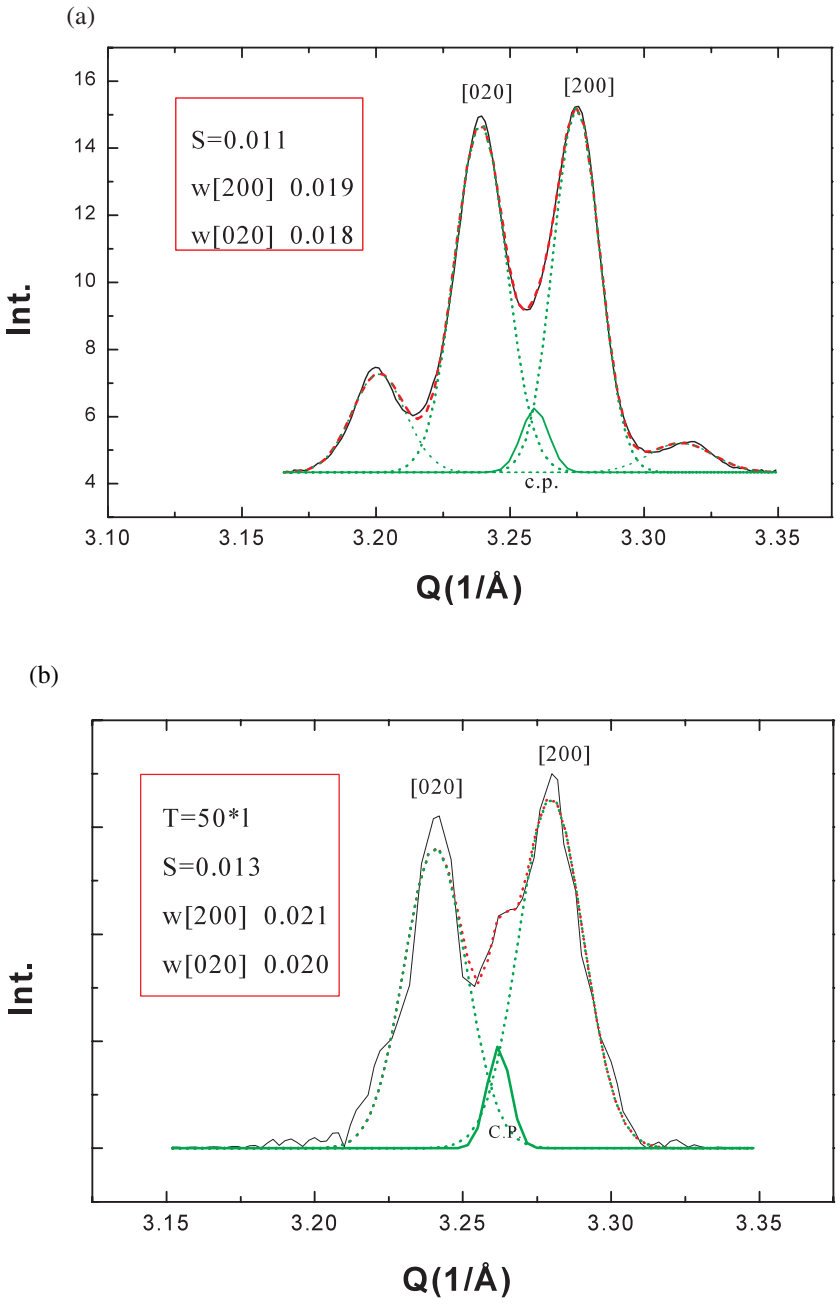

Figure 13. (a) The measured diffraction pattern for the [200] and [020] reflections fitted by Gaussian profile shape functions. A good fit requires the addition of a small central peak (c.p.) and yields $S = 0.011$ from the outer peaks. Here, the sample is equilibrated under 10 mbar oxygen p.p at 500 °C. w [200] shows the width of the [200] peak. (b) The calculated diffraction pattern for $S = 0.013$ and $T = 50$ in Q space (full curve), again fitted with Gaussian shape functions (dotted curves). A good fit requires the addition of a small central peak, comparable with the feature inferred from the diffracted data in (a). The oscillations in the calculated line are an artefact of the limited region simulated in real space. The peak widths of the calculated profile for the [200] and [020] peaks are given.

(c) The x dependence of the [h00] reflections is consistent with a model in which the width of twins increases with increasing orthorhombicity
(d) Variation in the [00l] reflections suggests that the appearance of the OI phase introduces significant strain in the c direction.
(e) By comparison of the simulated and real data, it is possible to estimate the widths of the twinned regions in their early stage of formation.

Acknowledgments

The authors would like to acknowledge the considerable assistance of ISIS staff in performance of the experiment, in particular Ken Anderson (the instrument scientist) and John Dreyer for help with the oxygen handling system. They would also thank Dr H Arabi (Iran) for his advice, Robin Thompson for help with running the XRD measurements in Salford and Michelle Mercer for advice on the experimental technique and for providing her data on the isotherms. B K would like to thank the Iranian Ministry of Higher Education for his scholarship. The authors would also like to thank the referee for extremely useful comments.

Note added in proof. We have recently come across a paper by J M Cowley and A Y Au (1978 *Acta Cryst.* A **34** 738–43) which provides an analytic expression for interference between diffraction from two adjacent microtwins. Morover, this approach has been used by F Zolliker, K Yvon and Ch Baerlocker (1986 *J. Less-Comm. Met.115* 65–78) in the analysis of microtwinning in the monoclinic structure of Mg_2NiH_4 where a 'central' peak is attributed to a similar effect. However, to the best of our knowledge, it has not previously been applied to YBCO.

References

[1] Civale L, Marwich A D, Worthington T K, Kirk M A, Thompson J R, Sun Y, Clem J R, Kursin-Elbaum L and Holtzberg F 1991 *Phys. Rev. Lett.* **67** 648
[2] Kwok W K, Welp U, Vinokur V M, Fleshler S, Downey J and Crabtree G W 1991 *Phys. Rev. Lett.* **67** 390
[3] Moodie A F and Whitfield H J 1988 *Ultramicroscopy* **24** 329
[4] David W I F, Moze O, Licci F, Bolzoni F, Cywinski R and Kilcoyne S 1989 *Physica* B **156** 880
[5] Zhu Y, Suenaga M and Tafto J 1993 *Phil. Mag.* A **67** 573
[6] Salje E and Parlinski K 1991 *Semicond. Sci. Technol.* **4** 93
[7] Schmhal W W, Putnis A, Salje E, Freeman P, Graeme-Barber A, Jones R, Singh K K, Blunt J, Edwards P P, Loram J and Mirza K 1989 *Phil. Mag. Lett.* **60** 241
[8] Xu Y, Suenaga M, Tafto J, Sabatini R L, Moodenbaugh A R and Zolliker P 1989 *Phys. Rev.* B **39** 6667
[9] Locherer K R, Hayward S A, Hirst P J, Ghrosch J, Yeadon M, Abell J S and Salje E K H 1996 *Phil. Trans. R. Soc.* A **354** 2815
[10] Gerdanian P and Picard C 1993 *Physica* C **204** 419
[11] Schleger P, Hardy W N and Yang B X 1991 *Physica* C **176** 261
[12] Mercer M 1996 A study of oxygen in the YBCO H-T_c superconducting material *PhD Thesis* University of Salford
[13] de Fontaine D, Wille L T and Moss S C 1987 *Phys. Rev.* B **36** 5709
[14] Wille L T, Berera A and de Fontaine D 1988 *Phys. Rev. Lett.* **60** 1065
[15] Salomons E and de Fontaine D 1990 *Phys. Rev.* B **42** 10152
[16] Schwarz W, Blaschko O, Collin G and Marucco F 1993 *Phys. Rev.* B **48** 6513
[17] Jorgensen J D, Veal B W, Paulikas A P, Nowicki L J, Crabtree G W, Claus H and Kwok W K 1990 *Phys. Rev.* B **41** 1863
[18] Rand M, Langford J I and Abell J S 1993 *Phil. Mag.* B **68** 17
[19] Khachaturyan A G 1983 *Theory of Structural Transformation in Solids* (New York: Wiley) ch 11
[20] Sarikaya M and Stern E A 1988 *Phys. Rev.* B **37** 9373
[21] Goncharov V A and Suvorov E V 1993 *The Real Structure of High-T_c Superconductors (Springer Series in Material Science vol 23)* ed V Sh Shekhtman (Berlin: Springer) ch 2
[22] Ross D K and Khoshnevisan B 2002 at press